



# Evaluation of Dynamic Mechanical Loading as an Accelerated Test Method for Ribbon Fatigue

## Preprint

Nick Bosco,<sup>1</sup> Timothy J. Silverman,<sup>1</sup> John Wohlgemuth,<sup>1</sup> Sarah Kurtz,<sup>1</sup> Masanao Inoue,<sup>2</sup> Keiichiro Sakurai,<sup>2</sup> Tsuyoshi Shioda,<sup>3</sup> Hirofumi Zenkoh,<sup>3</sup> Kusato Hirota,<sup>4</sup> Masanori Miyashita,<sup>4</sup> Tanahashi Tadanori,<sup>5</sup> and Satoshi Suzuki<sup>5</sup>

<sup>1</sup> *National Renewable Energy Laboratory*

<sup>2</sup> *National Institute of Advanced Industrial Science and Technology*

<sup>3</sup> *Mitsui Chemical*

<sup>4</sup> *Toray*

<sup>5</sup> *Espec*

*Presented at 29th European Photovoltaic Solar Energy Conference (EU PVSEC 2014)*

*Amsterdam, The Netherlands*

*September 22–26, 2014*

**NREL is a national laboratory of the U.S. Department of Energy  
Office of Energy Efficiency & Renewable Energy  
Operated by the Alliance for Sustainable Energy, LLC**

This report is available at no cost from the National Renewable Energy Laboratory (NREL) at [www.nrel.gov/publications](http://www.nrel.gov/publications).

**Conference Paper**

NREL/CP-5J00-62596

April 2015

Contract No. DE-AC36-08GO28308

## NOTICE

The submitted manuscript has been offered by an employee of the Alliance for Sustainable Energy, LLC (Alliance), a contractor of the US Government under Contract No. DE-AC36-08GO28308. Accordingly, the US Government and Alliance retain a nonexclusive royalty-free license to publish or reproduce the published form of this contribution, or allow others to do so, for US Government purposes.

This report was prepared as an account of work sponsored by an agency of the United States government. Neither the United States government nor any agency thereof, nor any of their employees, makes any warranty, express or implied, or assumes any legal liability or responsibility for the accuracy, completeness, or usefulness of any information, apparatus, product, or process disclosed, or represents that its use would not infringe privately owned rights. Reference herein to any specific commercial product, process, or service by trade name, trademark, manufacturer, or otherwise does not necessarily constitute or imply its endorsement, recommendation, or favoring by the United States government or any agency thereof. The views and opinions of authors expressed herein do not necessarily state or reflect those of the United States government or any agency thereof.

This report is available at no cost from the National Renewable Energy Laboratory (NREL) at [www.nrel.gov/publications](http://www.nrel.gov/publications).

Available electronically at <http://www.osti.gov/scitech>

Available for a processing fee to U.S. Department of Energy and its contractors, in paper, from:

U.S. Department of Energy  
Office of Scientific and Technical Information  
P.O. Box 62  
Oak Ridge, TN 37831-0062  
phone: 865.576.8401  
fax: 865.576.5728  
email: <mailto:reports@adonis.osti.gov>

Available for sale to the public, in paper, from:

U.S. Department of Commerce  
National Technical Information Service  
5285 Port Royal Road  
Springfield, VA 22161  
phone: 800.553.6847  
fax: 703.605.6900  
email: [orders@ntis.fedworld.gov](mailto:orders@ntis.fedworld.gov)  
online ordering: <http://www.ntis.gov/help/ordermethods.aspx>

*Cover Photos: (left to right) photo by Pat Corkery, NREL 16416, photo from SunEdison, NREL 17423, photo by Pat Corkery, NREL 16560, photo by Dennis Schroeder, NREL 17613, photo by Dean Armstrong, NREL 17436, photo by Pat Corkery, NREL 17721.*

# Evaluation of Dynamic Mechanical Loading as an Accelerated Test Method for Ribbon Fatigue

Nick Bosco<sup>1</sup>, Timothy J Silverman<sup>1</sup>, John Wohlgemuth<sup>1</sup>, Sarah Kurtz<sup>1</sup>, Masanao Inoue<sup>2</sup>, Keiichiro Sakurai<sup>2</sup>, Tsuyoshi Shioda<sup>3</sup>, Hirofumi Zenkoh<sup>3</sup>, Kusato Hirota<sup>4</sup>, Masanori Miyashita<sup>4</sup>, Tanahashi Tadanori<sup>5</sup>, Soh Suzuki<sup>5</sup>, Yifeng Chen<sup>6</sup> and Pierre J. Verlinden<sup>6</sup>

<sup>1</sup>NREL, Golden, CO, USA, <sup>2</sup>National Institute of Advanced Industrial Science and Technology (AIST), Japan, <sup>3</sup>Mitsui Chemical, <sup>4</sup>Toray, <sup>5</sup>Espec, <sup>6</sup>State Key Laboratory of PV Science and Technology, Trina Solar

**ABSTRACT** — **Dynamic Mechanical Loading (DML) of photovoltaic modules is explored as a route to quickly fatigue copper interconnect ribbons. Results indicate that most of the interconnect ribbons may be strained through module mechanical loading to a level that will result in failure in a few hundred to thousands of cycles. Considering the speed at which DML may be applied, this translates into a few hours of testing. To evaluate the equivalence of DML to thermal cycling, parallel tests were conducted with thermal cycling. Preliminary analysis suggests that one  $\pm 1$  kPa DML cycle is roughly equivalent to one standard accelerated thermal cycle and approximately 175 of these cycles are equivalent to a 25-year exposure in Golden Colorado for the mechanism of module ribbon fatigue.**

## I. INTRODUCTION

Interconnect ribbon failure is a common failure mode in flat plate photovoltaic modules. The driving force for this type of failure is fatigue originating from both thermal and mechanical induced strain [1-3]. Currently the IEC 61215 Design Qualification and Type Approval standard addresses this mechanism with an accelerated test of thermal cycling ( $-40$  to  $85^\circ\text{C}$ , 200 cycles), which has been previously reported as equivalent to  $\sim 10$  years of outdoor exposure [4, 5]. A direct measurement of an acceleration factor between thermal cycling and/or mechanical loading, and outdoor exposure, however, is absent. To assess long-term reliability, commensurate with module warranty periods of 20–30 years, these relationships must be quantified.

We assess Dynamic Mechanical Loading (DML) as a method to evaluate interconnect reliability. Unlike solder fatigue, the fatigue mechanism in interconnect ribbon is independent of both time and temperature and can therefore be activated by quickly loading the module. Ribbon fatigue damage is accumulated with every loading cycle and only depends on the size of each cycle and the number of cycles. Larger strains impart exponentially more fatigue damage; therefore many small loading cycles may be easily, and predictably, replaced with fewer large cycles. This phenomenon of ribbon fatigue allows for a straightforward correlation between service and accelerated test conditions.

In this paper the extent of ribbon strain with loading is measured. The conditions of loading level and forward bias are explored for their effect on ribbon strain and failure rate during DML testing. A Finite Element Model (FEM) is created to assess how module size and aspect ratio affect DML induced ribbon strain. Finally, parallel experiments of DML testing and thermal cycling are then conducted to find the equivalency between the two methods and outdoor exposure.

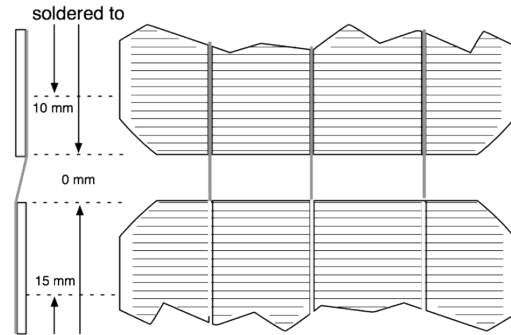


Fig. 1. Cartoon illustrating the point to which the interconnect ribbon is soldered on each cell for the offset and no-offset modules.

## II. MATERIALS AND METHODS

### A. Materials

42-cell 1 x 1.2 m flat-plate glass/polymer backsheets crystalline silicon modules with an aluminum frame were fabricated by The National Institute of Advanced Industrial Science and Technology (AIST) for the purpose of this study. Two stringing schemes were used to fabricate the modules: one where the front-side interconnect ribbons were soldered to 10 mm from the cells' edges and the backside interconnect to 15 mm (offset) and one where both the front and backside connections were soldered to the cells' edges (no-offset), Fig. 1. The effective gage length of the interconnect ribbons soldered to the cells edge is 25 mm shorter than for the offset case, and therefore expected to experience proportionally more strain for similar amounts of cell-to-cell deflection. This scheme was intentionally included in this study to provide for a poorly designed module that should fail more quickly.

### B. Measurements

For the DML testing, the back of the module was sealed such that a positive or negative gage pressure of air could be applied to its underside, thereby imparting a uniform load across its area. The load was varied from  $-3$  to  $+3$  kPa while the cell-to-cell spacing was measured optically by imaging the gap between cells. Each image was digitally analyzed to quantify the change in spacing with applied load. Cell-to-cell strain, Eq (1), is calculated in the following way:

$$\varepsilon = \frac{(du_L - du_o)}{du_o} \cdot 100\%, \quad (1)$$

where  $du_L$  and  $du_o$  are the loaded and unloaded in-plane distance between adjacent cells.

The out-of-plane deflection of the module's front glass surface was measured between a stiff beam affixed across the module and the deflecting glass surface with a position sensor. Multiple positions across the glass's surface were measured while the load was varied from  $-3$  kPa to  $+3$  kPa.

### C. Module Characterization and Testing

Prior to testing, each module was imaged for its electroluminescence emission under  $I_{sc}$  forward bias conditions (9 A,  $\sim 28$  V). The test modules were then subjected to either DML or thermal cycling according to Table 1 and as described below.

	Dynamic Mechanical Loading			Thermal Cycling
	3 kPa w/bias	3 kPa	1.5 kPa w/bias	
no-offset	2	2	2	2
offset	2	2	2	2

Table 1. DML and thermal cycling testing matrix

Two levels of DML testing were conducted at cyclic loads of  $\pm 3$  kPa and  $\pm 1.5$  kPa. At the higher loading level, tests were conducted both with and without the application of forward current bias, while, at the lower loading level, only one test condition with forward bias was conducted. At intervals of 1000 cycles the modules were removed from testing and imaged by electroluminescence under  $I_{sc}$  forward bias conditions.

The modules tested under  $I_{sc}$  forward bias conditions were also monitored for in-situ changes in differential conductance ( $dG$ ). With the module under forward bias, a sinusoidal voltage signal with peak-to-peak amplitude of 100 mV was applied at 1 kHz and the resulting RMS voltage and current recorded. Changes in the  $dG$  ( $I_{rms}/V_{rms}$ ) were expected to correspond with changes in the module's series resistance, or ribbon failure.

The thermal cycling sequence according to IEC 61215 was conducted on two each of the no-offset and offset modules. The cycle parameters were three-hour cycles from  $-40$  to  $85^\circ\text{C}$  with 10 min dwells (ramp rate  $\sim 1.5^\circ\text{C}/\text{min}$ ). The modules' electrical characteristics are measured and electroluminescence emission imaged every 200 cycles.

### D. Finite Element Modeling

A finite-element model of the module to predict ribbon strain and out-of-plane module deflection for a given loading scenario was developed. The model includes the front glass, encapsulant, cells and two-layer backsheets, using material properties provided by the component manufacturers. Materials are assumed to have temperature-dependent, linear-elastic constitutive behavior. The interconnect ribbons are assumed not to affect the cell-to-cell spacing or out-of-plane deflection and are omitted from the model. The aluminum frame is approximated as a spring foundation acting at the margin of the glass. The model includes one quarter of the module to take advantage of symmetry.

Air pressure is simulated by the application of uniform pressure on the backsheets surface. Because the laminate undergoes large deflections, the model is solved with geometric nonlinearity taken into account, ensuring that the pressure is applied normal to the deflected module surface.

## III. RESULTS AND ANALYSIS

### A. Measurements and Simulations

Plots of measured and simulated module deflection are presented in Fig. 2. Because of the modules' two axes of symmetry, only one quarter of the module is depicted with the origin at the center of the module and abscissa and ordinate representing the center and mid-line axes of symmetry. These plots illustrate the out-of-plane deflection of the module front glass whilst loaded at  $-3$  kPa and show measurement and simulation in good agreement. Under this loading condition the front glass bows downward, creating a concave surface, thus the negative deflection values. Measurements made while the module was at  $I_{sc}$  forward bias conditions resulting in a front surface glass temperature of approximately  $37^\circ\text{C}$  yielded deflection values within the error of measurement to the un-biased condition.

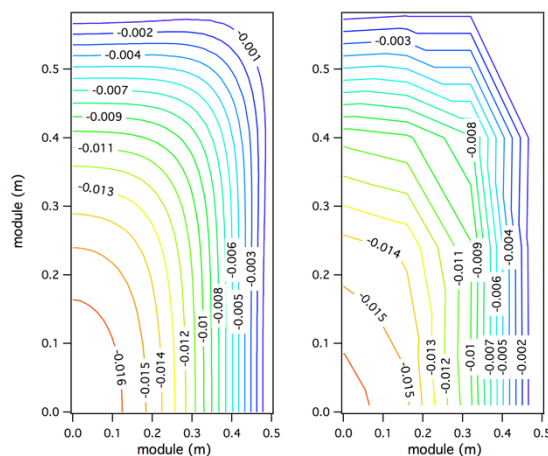


Fig. 2. Contour plots of simulated (left) and measured (right) module deflection under  $-3$  kPa loading. Plot origins are located at the middle of the module and the abscissa and ordinate represent the two axis of symmetry. Contours are labeled with module deflection in m.

Plots of measured and simulated cell-to-cell strain versus applied load for each of the unique cell connections are presented in Fig. 3. Included in the figure are diagrams that describe between which strung cells the strain is being reported. The most cell-to-cell strain occurs at the top and bottom of the module, and more so in the center. The non-symmetric strain with reverse loading is captured well by the FEM. Even the negative strain with both positive and negative loading that occurs at the center edges of the module are correctly predicted by the model. An additional set of strain measurements taken while the module was forward biased at its short circuit current is presented in Fig. 4.

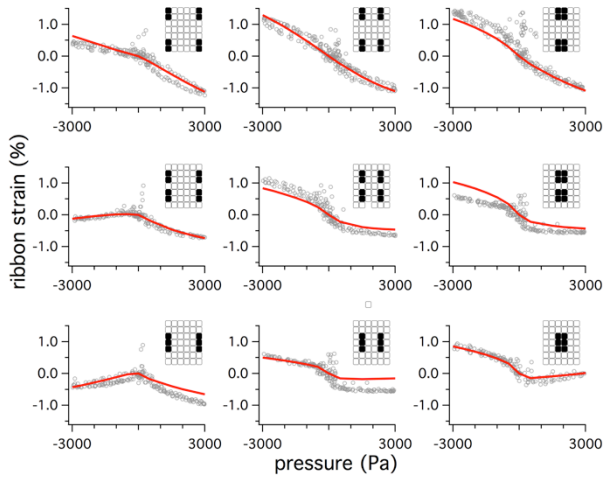


Fig. 3. Plots of measured cell-to-cell strain with module loading at room temperature (open symbols) and model results (solid line). Inset diagrams illustrate between which adjacent strung cells the strain is reported.

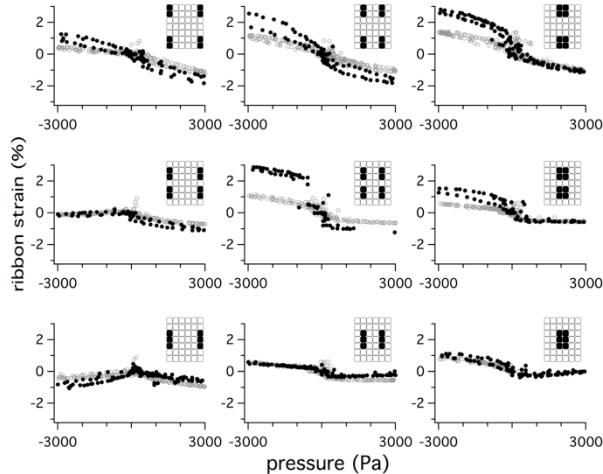


Fig. 4 Plots of measured cell-to-cell strain with module loading at room temperature (open symbols) and while forward biased at short circuit current (closed symbols). Inset diagrams illustrate between which adjacent strung cells the strain is reported.

Under these conditions the front glass of the module was 37°C and the strain amplitude measured is greater primarily in the center of the module when compared to the room temperature measurements. Considering that elevating the temperature of the module did not increase the amount of front glass deflection, the additional ribbon strain is likely due to the softening encapsulant reducing the cell constraint.

Most relevant to its potential as a driving force for ribbon fatigue (in place of thermal cycling) is the strain amplitude achieved through the mechanical application of cyclic loading, shown in Fig. 5. For the loading level of  $\pm 3$  kPa on the unbiased module, 5 of the 9 locations experience strain amplitude of over 1.5%. For the biased module, the maximum strain amplitude increases to over 4%.

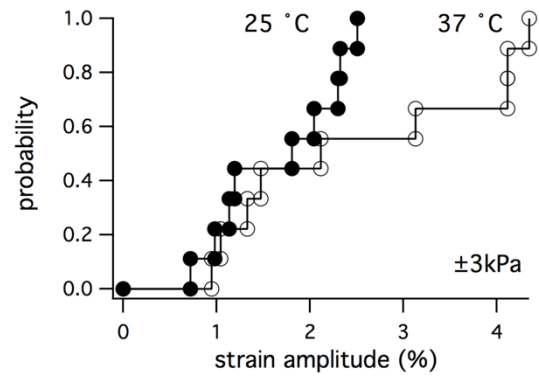


Fig. 5 Cumulative Distribution Plot of measured cell-to-cell strain amplitude for the  $\pm 3$  kPa loading condition at room temperature (closed symbols) and while under forward bias (open symbols).

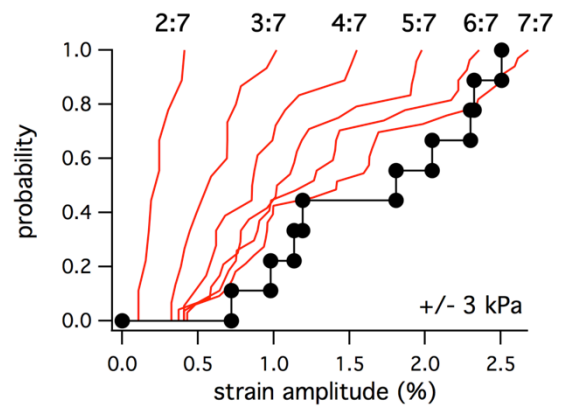


Fig. 6 Cumulative Distribution Plot of simulated cell-to-cell strain amplitude for the  $\pm 3$  kPa loading condition at room temperature (closed symbols) and dependence of strain amplitude on module aspect ratio.

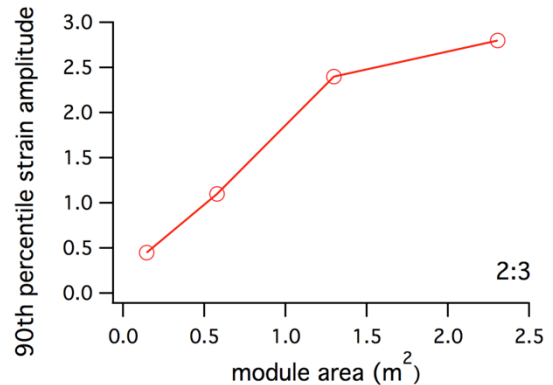


Fig. 7 Simulated 90<sup>th</sup> percentile ribbon strain as a function of module area for a fixed 2:3 cell aspect ratio.

The FEM was used to explore the effect of module size and aspect ratio on the magnitude and distribution of ribbon strain. Aspect ratios from 2:7 to 7:7 (square) cells were simulated for a loading condition of  $\pm 3$  kPa and the module size dictated by

the 155 mm cell size. The results of the simulations are plotted in the form of a cumulative distribution function (CDF) along with the measured values of our test module (6:7 ratio), Fig. 6. The results indicate that the lower aspect ratio modules (more square) demonstrate a larger population of higher strain amplitudes. Also evident is a strong correlation between aspect ratio and strain amplitude distribution. The effect of module area on ribbon strain distribution was also explored with the FEM. The results of our simulations are presented as the 90<sup>th</sup> percentile ribbon strain vs. module area for a fixed 2:3 cell aspect ratio, Fig. 7, and indicate larger strains are achieved as the module area increases. Considering the multitude of module sizes, this type of analysis is critical in designing an equitable DML test procedure.

### B. DML Testing

The results of all DML tests are summarized in a cumulative failure plot, Fig. 8. The open symbols represent the offset modules and the closed symbols the no-offset modules. The ribbon failure rate of the no-offset modules is accelerated compared to the offset modules. The modules at the higher loading condition also exhibit the expected faster failure rate than the modules at the lower loading condition. Without the application of forward bias, the  $dG$  cannot be monitored during the un-biased DML test and therefore the evaluation of ribbon fatigue was only made at the testing intervals of 1000 cycles by EL imaging. Due to the lower temperature and therefore lower level of strain, this module exhibited the slowest failure rate despite the high loading level. This is consistent with the previous observation that a higher level of strain is achieved for a given loading level when the module is at an elevated temperature.

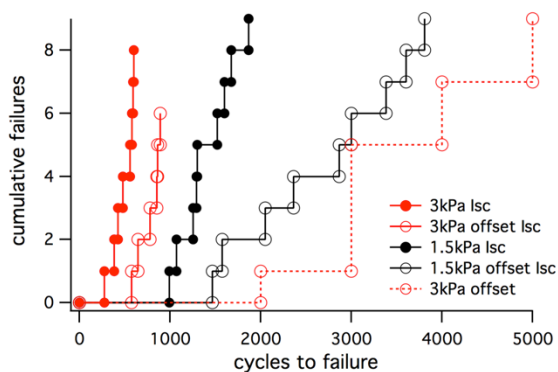


Fig. 8 Cumulative failure plot for all modules. Both modules with ribbon offset (open symbols) and no ribbon offset (closed symbols) are presented along with the unbiased module (dashed line).

The failure data presented in Fig. 8 for the biased modules were used to construct an S-N plot which describes the relationship between strain amplitude (S) and number of cycles to failure (N), Fig. 9. The strain amplitude reported is from the forward biased strain measurements presented in

Fig. 4. The data are fit according to *Basquin's Law*, an empirical power law equation found to fit high-cycle fatigue failure,

$$\Delta\varepsilon = \varepsilon_p N_f^c \quad (2)$$

where  $\Delta\varepsilon$  is the strain amplitude,  $N_f$  the number of cycles to failure and  $\varepsilon_p$  and  $c$  fitting constants ( $\varepsilon_p = 21.14$ ;  $c = -0.29$ ) [6]. Considering the DML test modules reached higher temperatures than the module evaluated for the strain measurements, the actual strain levels may be higher which would shift the curve up and/or result in a steeper slope. The accelerated failure rate of the modules with no-offset is represented by the black dashed line in Fig. 8 and simply signifies failures occurring 40% faster as roughly measured from Fig. 8. The purpose of presenting this S-N curve is to demonstrate how fatigue failures experienced in one regime of strain may be predictably extrapolated to another.

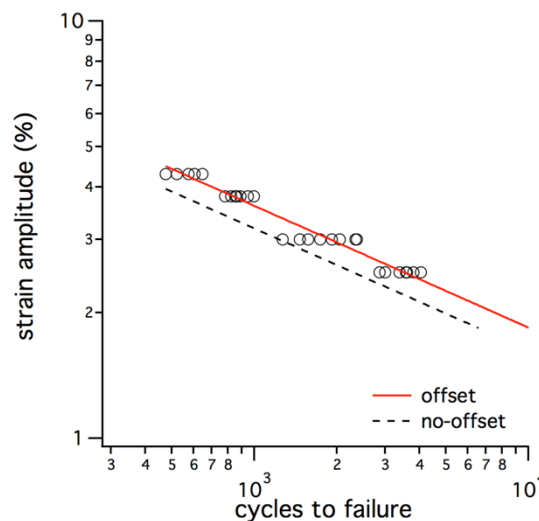


Fig. 9 S-N curve and power law fit to fatigue failures of the forward biased DML tested modules.

### C. Thermal Cycling

An optical measurement of ribbon strain through temperature cycling was made to compare to the strain imparted through mechanical loading, Fig. 10. It was found that a ribbon strain amplitude of  $\sim 2.5\%$  is experienced for a temperature change from  $-20$  to  $85^\circ\text{C}$ . This result is consistent with a more rigorous experiment conducted by Meier, et al [7]. According to their empirical model, a temperature change of  $125^\circ\text{C}$  ( $-40$  to  $85^\circ\text{C}$ ) yields a strain change of  $2.9\%$ . Referring to Fig. 4, this level of strain amplitude is also achieved with a loading condition of  $\pm 1$  kPa for several locations across the module. This observation suggests the DML loading level of  $\pm 1$  kPa yields a similar acceleration factor for ribbon fatigue as the IEC qualification level thermal cycling. At the time of manuscript submission, the thermal cycling sequence had been evaluated through 3000 cycles for the offset modules and 1000 cycles for the no-

offset modules with only one early ribbon failure detected. According to the S-N plot in Fig. 9, failures for the offset modules are not expected until ~3700 cycles and ~2400 cycles for the no-offset modules.

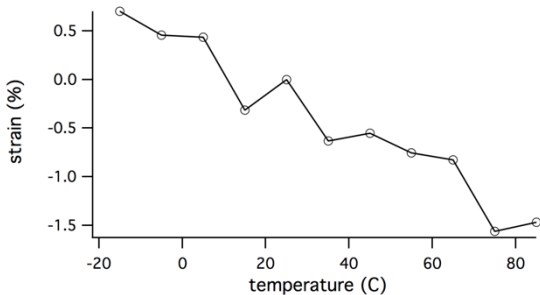


Fig. 10 Module ribbon strain vs. module temperature.

Knowledge of the S-N relationship for ribbon fatigue in modules also provides for a method to calculate an acceleration factor between accelerated testing and service. Damage is defined as  $N/N_f$  where  $N$  is the number of cycles completed at the level which defines  $N_f$ , so that once the accumulated damage reaches unity, failure will occur. To consider cycles of various strain amplitudes, we may simply sum their damages. By realizing strain amplitude is a function of temperature change we achieve:

$$D = \sum \frac{1}{N_f} = \sum \left( \frac{\Delta\epsilon(\Delta T)}{\epsilon_p} \right)^{-\frac{1}{c}} \quad (3)$$

One year of weather data from Golden, Colorado, in one-minute intervals, was converted to module temperature using an exponentially weighted average of the King temperature equation, as described in detail elsewhere [8, 9]. This history of temperature was then converted into a series of temperature changes and evaluated by Eq (3) three ways: (TC) considering every temperature change encountered, (RFC) considering those temperature changes identified by the rainflow algorithm, and (DC) considering only the maximum temperature change experienced each day. The rainflow algorithm attempts to remove smaller temperature reversals that occur within larger ones, so as to not segment the larger cycle into smaller, less damaging, ones [8]. The results of these calculations for the year are presented in Fig. 11 and normalized by the amount of ribbon fatigue damage imparted by one IEC qualification thermal cycle or one  $\pm 1$  kPa DML cycle.

The figure illustrates that the approach using the maximum change for each day is most conservative, which is an artifact of the power law equation for damage. With this most conservative approach, one-year exposure in Golden, Colorado is calculated to be equivalent to roughly seven cycles. This acceleration factor gives a 25-year exposure in 175 cycles, which is within the qualification level of 200 thermal cycles and well within proposed DML test sequences that include 1000 cycles of  $\pm 1$  kPa loading.

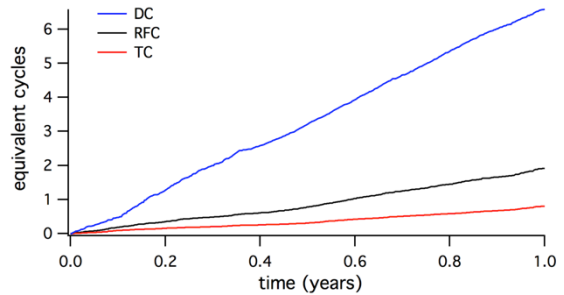


Fig. 11 Plot of module ribbon fatigue damage over one year exposure in Golden, Colorado, normalized to IEC qualification level thermal cycles when counting every temperature change (TC), only those changes identified by the rainflow algorithm (RFC) and the maximum change each day (DC).

## VI. CONCLUSIONS

The current work has demonstrated that mechanical loading of a PV module reproducibly induces interconnect ribbon strain sufficient to cause fatigue failures. Our measurements of ribbon strain with mechanical loading across a module and their corresponding fatigue failure rates have allowed us to produce an S-N plot for module ribbon fatigue. This plot describes the relationship between module ribbon strain amplitude and the number of fatigue cycles required to cause failure. The S-N plot also highlights how, unlike thermal cycling, module mechanical loading imparts a distribution of ribbon strains across the module. This distribution was found to depend on factors such as ribbon location, loading pressure, module size, aspect ratio, temperature and laminate properties. Through FEM simulations, we have begun to demonstrate an understanding of these relationships as a first step towards defining an equivalent test for a module of any character.

Characterization of the S-N relationship for module ribbons has also allowed us to correlate mechanical loading to thermal cycling induced fatigue failures. We have calculated that the acceleration factor between  $-40$  to  $85^\circ\text{C}$  thermal cycles and  $\pm 1$  kPa DML cycles is roughly one and 25 years of exposure in Golden, Colorado is equivalent to approximately 175 of these cycles. While DML testing has been demonstrated as a much faster analogue for thermal cycling to evaluate interconnection ribbon fatigue, it cannot similarly evaluate solder fatigue. Solder fatigue is both a temperature and time dependent process that is not similarly activated by fast mechanical loading cycles.

## VI. ACKNOWLEDGEMENTS

This work was supported by the U.S. Department of Energy under Contract No. DE-AC36-08-GO28308 with the National Renewable Energy Laboratory.

## REFERENCES

- [1] L. N. Dumas and A. Shumka, "Photovoltaic Module Reliability Improvement through Application Testing and Failure Analysis," *Reliability, IEEE Transactions on*, vol. R-31, pp. 228-234, 1982.
- [2] M. I. Smokler, D. H. Otth, and R. G. Ross, "The Block program approach to photovoltaic module development," in *Proceedings of the 18th IEEE PV Specialists Conference*, Las Vegas, Nevada, USA, 1985, pp. 1150-1158.
- [3] M. I. Smokler, "Block V module development and test results," in *Proceedings of the 6th European Commission PV Solar Energy Conference*, London, UK, 1985, pp. 370-376.
- [4] J. H. Wohlgemuth, "Testing for Module Warranties," presented at the Photovoltaic Performance and Reliability Workshop, 1983.
- [5] J. H. Wohlgemuth, "Reliability testing of PV modules," in *Proceedings of the 1st World Conference on PV Energy Conversion*, Waikoloa, Hawaii, USA, 1994, pp. 889-892.
- [6] P. Paris and F. Erdogan, "A Critical Analysis of Crack Propagation Laws," *Journal of Basic Engineering, Transactions of the American Society of Mechanical Engineers*, pp. 528-534, December 1963.
- [7] R. Meier, F. Kraemer, S. Wiese, K. Wolter, and J. Bagdahn, "Reliability of copper-ribbons in photovoltaic modules under thermo-mechanical loading," in *Photovoltaic Specialists Conference (PVSC), 2010 35th IEEE*, 2010, pp. 001283-001288.
- [8] N. Bosco and S. Kurtz, "Quantifying the Thermal Fatigue of CPV Modules," *AIP Conference Proceedings*, vol. 1277, pp. 225-228, 2010.
- [9] D. L. King, W. E. Boyson, and J. A. Kratochvil, "Photovoltaic array performance model," Sandia National Laboratories SAND2004-3535, 2004.